Electronic Supplementary Material (ESI) for Journal of Materials Chemistry A.

Narrow band gap and high mobility of lead free perovskite single crystals Sn-doped $MA_3Sb_2I_9$

Dianxing Ju,[a] *Xiaomei Jiang,*[a] *Hang Xiao,**[b,c] *Xi Chen,*[b,c] *Xiaobo Hu,*[a] *Xutang Tao**[a]

[a] State Key Laboratory of Crystal Materials, Shandong University No. 27 Shanda South Road, Jinan, 250100 (P.R. China)

E-mail: txt@sdu.edu.cn.

[b] Yonghong Zhang Family Center for Advanced Materials for Energy and Environment, Department of Earth and Environmental Engineering, Columbia University, New York, NY 10027, USA

[c] School of Chemical Engineering, Northwest University, Xi'an 710069, China

E-mail: hx2152@columbia.edu

Experimental Section

Materials: Analytical-grade reactants of $SbCl_3$, Methylamine hydrochloride ($CH_5N.HCl$), H_3PO_2 solution and HI solution were purchased from Sinopharm Co. Ltd. and used without further purification. Crystal growth of Sn-doped $MA_3Sb_2I_9$ as follows: Methylamine hydrochloride ($CH_5N.HCl$), $SbCl_3$ and SnO with the moral ratio of 4:2:1, were dissolved in a solution of HI and then transferred into Teflon-lined stainless steel autoclaves. After the reaction at 220 °C for 24 h with a cooling rate of 5 $^oC/h$, the Sn-doped $MA_3Sb_2I_9$ single crystals were successfully obtained. With the same process, we got the single crystal of $MA_3Sb_2I_9$, $MA_3Bi_2I_9$ and Sn-doped $MA_3Bi_2I_9$ single crystals.

X-Ray Diffraction: X-ray powder diffraction (XRD) patterns of polycrystalline powder were carried out on a Bruker-AXS D8 Advance X-ray diffractometer with CuKα1 radiation (λ = 1.54186 Å) in the range of 10-90° (2θ) with a step size of 0.004°. Single crystals' structures were determined by Bruker SMART APEX-II diffractometer equipped with a CCD detector (graphite-monochromatized Mo-Kα radiation, λ= 0.71073 Å) at 296 K. Data integration and cell refinement were performed using the APEX3 software. The structure was analysed by direct methods and refined using the SHELXTL 97 software package. All nonhydrogen atoms of the structure were refined with anisotropic thermal parameters, and the refinements converged for $Fo^2 > 2\sigma IJFo^2$. All the calculations were performed using SHELXTL crystallographic software package.] Symmetry analysis on the model using PLATON revealed that no obvious space group change was needed. In the refinement, the commands EDAP and EXYZ were used to restrain some of the related bond lengths and bond angles.

UV-vis-NIR diffuse reflectance spectra measurements: UV-vis-NIR diffuse reflectance spectroscopy was carried out using a Shimadzu UV 2550 spectrophotometer equipped with an integrating sphere over the spectral range 200-1500 nm. The $MA_3Sb_2I_9$ and the Sn-doped $MA_3Sb_2I_9$ single crystals were dried and ground into powders, as well as the $MA_3Bi_2I_9$ and the Sn-doped $MA_3Bi_2I_9$. A $BaSO_4$ plate was used as the standard (100% reflectance). The absorption spectrum was calculated from the reflectance spectrum using the Kubelka-Munk function: $\alpha/S= (1-R)^2/(2R)$, where α is the absorption coefficient, S is the scattering coefficient, and R is the reflectance.

SCLC and Hall Effect measurements: All current–voltage measurements were carried out by Keithley 2400 semiconductor parameter analyser. The dielectric

constant was measured by an Agilent 4294A impedance network analyzer, combined with the equation of $\varepsilon=Cpt/A\varepsilon_0$. Where Cp, t, ε, ε_0 and A are the capacitance, the thickness of single crystals, relative dielectric constant and the area of single crystals. The $MA_3Sb_2I_9$ and the Sn-doped $MA_3Sb_2I_9$ single crystals were about 2.64×3.1×0.53 mm^3 and 3.43×4.00×0.801 mm^3, respectively. Moreover, the $MA_3Bi_2I_9$ and the Sn-doped $MA_3Bi_2I_9$ single crystals were about 2.78×2.0×1.08 mm^3 and 1.53×3.17×0.88 mm^3, respectively. All of them were deposited the gold film as the electrodes on the two sides. The single crystals of $MA_3Sb_2I_9$ and the Sn-doped $MA_3Sb_2I_9$ with the thickness of about 0.41 mm and 0.65 mm were used for the measurements of Hall Effect. All of them were deposited with silver paste as the electrodes. The resistivity and the carrier concentration measurements were performed at room temperature on a 4-probe sample holder placed between the plates of an electromagnet on Ecopia HMS-5000 instrument. The magnetic field intensity was at 0.5 T.

Scanning electron microscope (SEM) measurement: The morphology microstructure of Sn-doped $MA_3Sb_2I_9$ single crystals was measured by a field emission scanning electron microscope (FESEM, FEI QUANTA FEG250).

Thermogravimetric analysis Measurements: Differential scanning calorimetry (DSC) and thermogravimetric analysis (TGA) were carried out using a TGA/DSC1/1600HT analyser (METTLER TOLEDO Instruments). The samples were placed in a platinum crucible, and heated at a rate of 10 °C min-1 from room temperature to 800 °C under flowing nitrogen gas. Differential scanning calorimetry (DSC) measurements were implemented on a NETZSCH DSC 200F3 analyser. The samples were placed in an aluminum crucible with the heating and cooling rates as 5 K/min from -120 K to 400 K in flowing nitrogen.

Density functional theory: Density functional theory (DFT)[1,2] calculations were performed with the using the ab initio code QUANTUM-ESPRESSO.[3] The Perdew-Burke-Ernzerh of (PBE)[4] of the generalized gradient approximation (GGA) was used for exchange-correlation functional. Electron-ion interactions were described by ultrasoft pseudopotentials, and a plane-wave cutoff energy of 80 Ry was used. Because GGA level DFT[5,6] is known to underestimate the band gaps of semiconductors, band structures of $(MA)_3Sb_2I_9$ crystal with or without Sn doping were calculated with HSE06 hybrid functional,[7] which has been demonstrated to be capable of predicting accurate band structures and density of states (DOS).[8] A 6×6×3 Monkhorst-Pack k-point grids (Γ point centered) was used for Brillouin zone sampling.[9] The conjugate gradient method (CG) was adopted to optimize the atomic

positions until the change in total energy was smaller than 5 $\times 10^{-6}$ eV/atom, maximum Hellmann–Feynman force within 0.01 eV $Å^{-1}$, and maximum stress within 0.005 GPa.

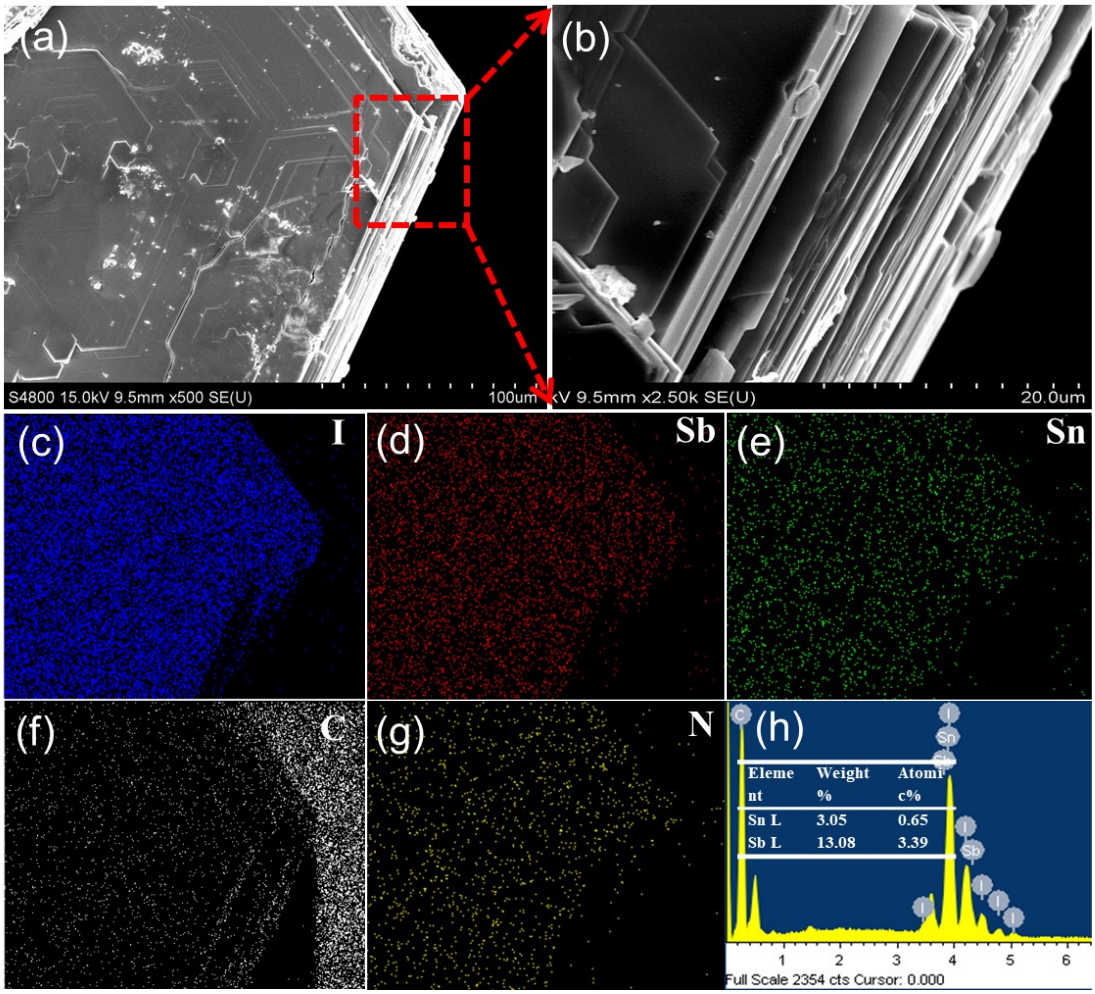

Fig. S1 (a, b) SEM images of the Sn-doped $MA_3Sb_2I_9$ single crystal. (c-g) Mapping images of different elements. (h) The corresponding EDS spectra of the single crystal shown in (a, b).

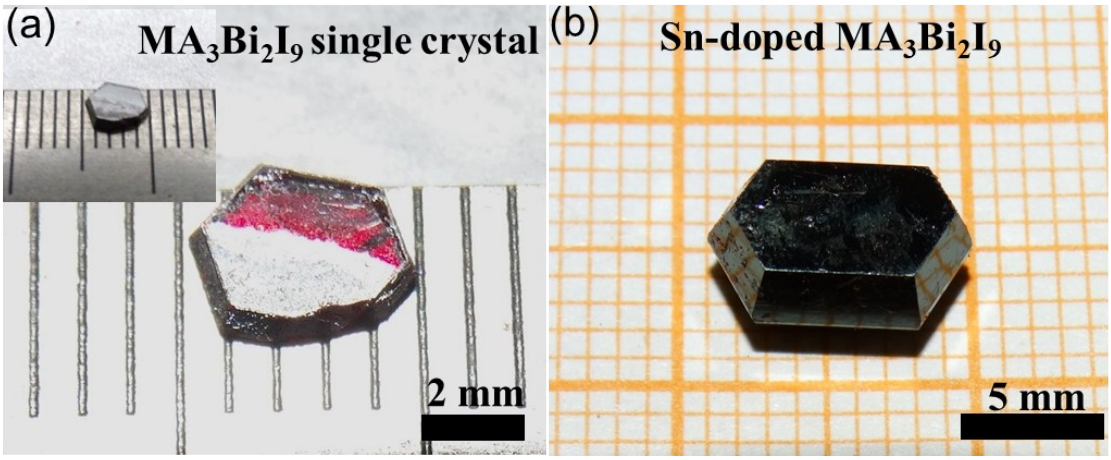

Fig. S2 Single crystals obtained by hydrothermal process. (a-b) $MA_3Bi_2I_9$, (c-d) Sn-doped $MA_3Bi_2I_9$.

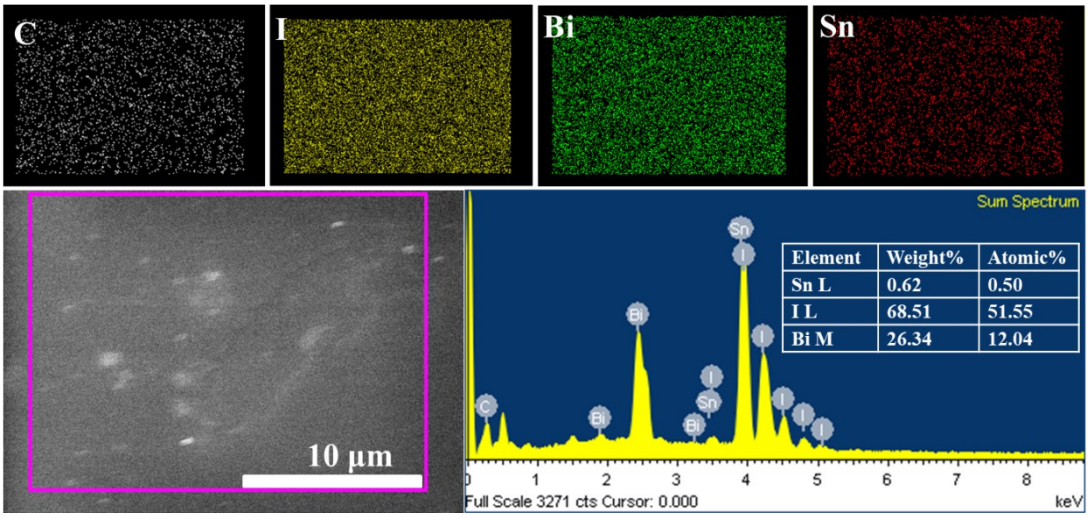

Fig. S3 Mapping images of the different elements and the corresponding EDS spectra of the Sn-doped $MA_3Bi_2I_9$ single crystal.

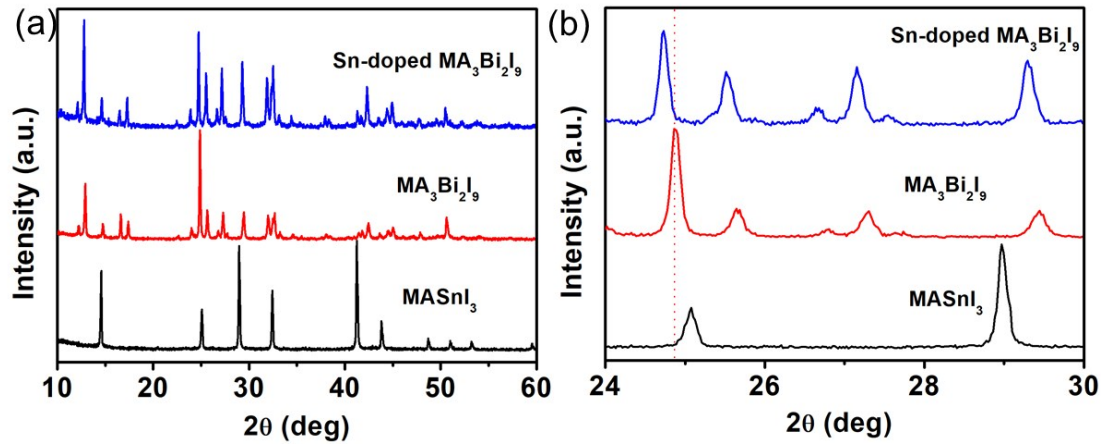

Fig. S4 (a) Experimental powder X-ray diffraction patterns for $MASnI_3$, $MA_3Bi_2I_9$ and Sn-doped $MA_3Bi_2I_9$ powder. (b) Local powder XRD patterns of the samples taken from (a).

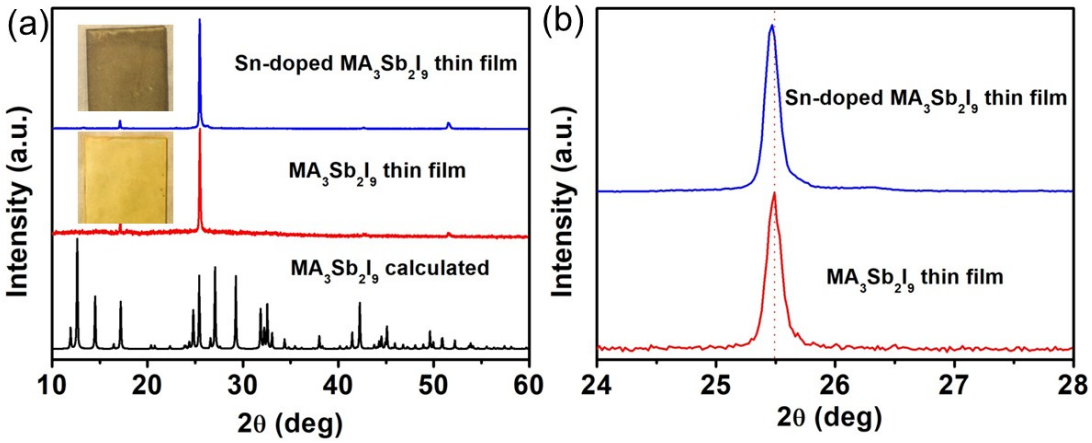

Fig. S5 X-ray diffraction patterns of $MA_3Sb_2I_9$ and Sn-doped $MA_3Sb_2I_9$ thin film.

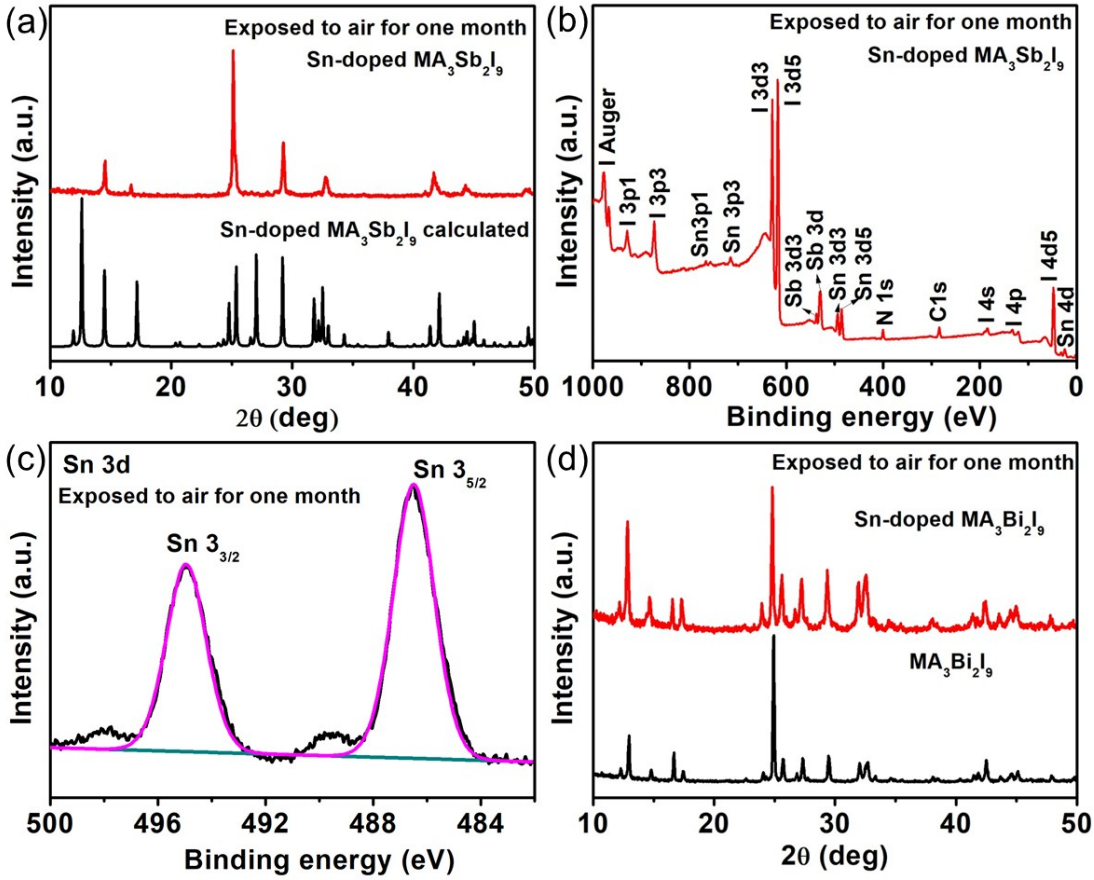

Figure S6. (a) Experimental and calculated powder X-ray diffraction patterns for Sn-doped $MA_3Sb_2I_9$ powder after exposed to air for one month. X-ray photoelectron spectra of Sn-doped $MA_3Sb_2I_9$ single crystal after exposed to the air for one month. (e) XPS full survey spectrum, (d) Sn 3d spectrum. (d) The powder XRD patterns of the $MA_3Bi_2I_9$ and Sn-doped $MA_3Bi_2I_9$ powder after exposed to air for one month.

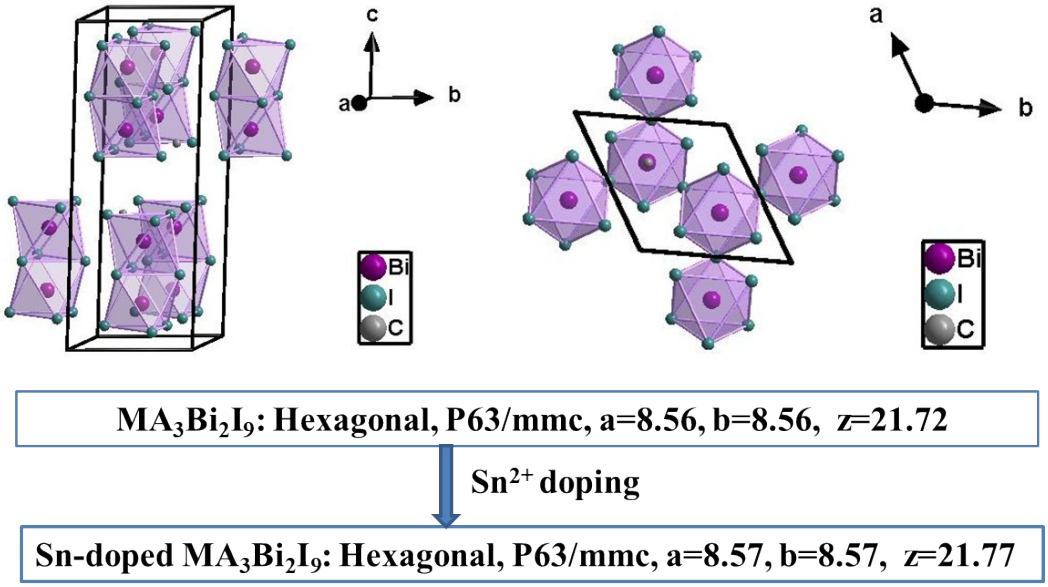

Fig. S7 Ball-and-stick diagrams of $MA_3Bi_2I_9$ and Sn-doped $MA_3BI_2I_9$ single crystals with the same structure. The C and N elements represent the disordered CH_3NH_3 groups; hydrogen atoms bonded to the C or N atoms were omitted for clarity.

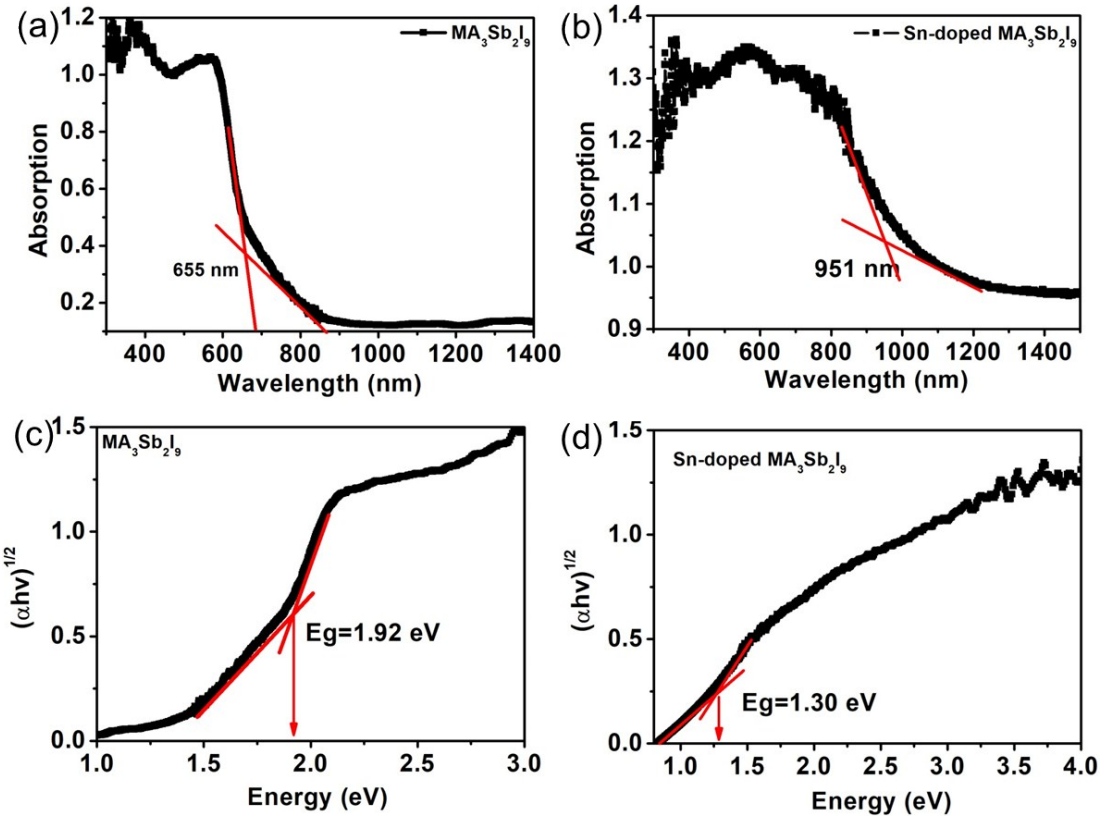

Fig. S8 (a, b) UV-vis diffuse reflectance spectroscopy plots for the $MA_3Sb_2I_9$ and Sn-doped $MA_3Sb_2I_9$. (c, d) Tauc plot analysis of the samples.

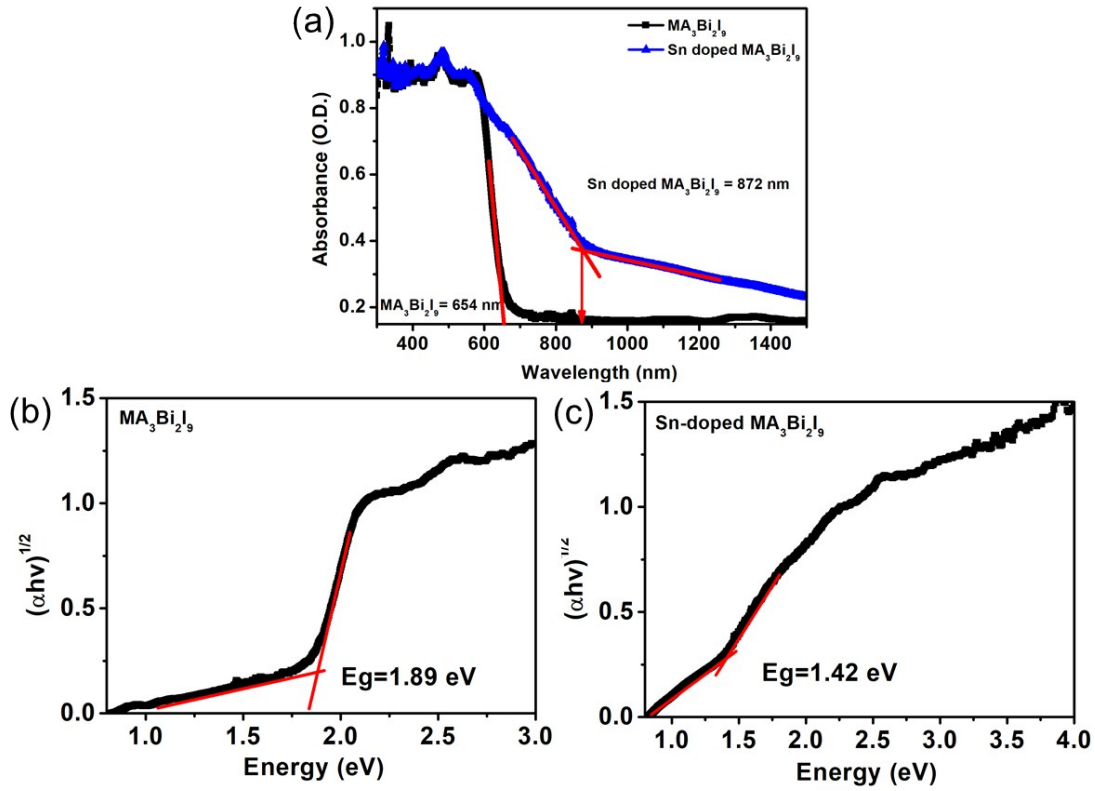

Fig. S9 (a) UV-vis diffuse reflectance spectroscopy plots for the $MA_3Bi_2I_9$ and Sn-doped $MA_3Bi_2I_9$. (b, c) Tauc plot analysis of the samples.

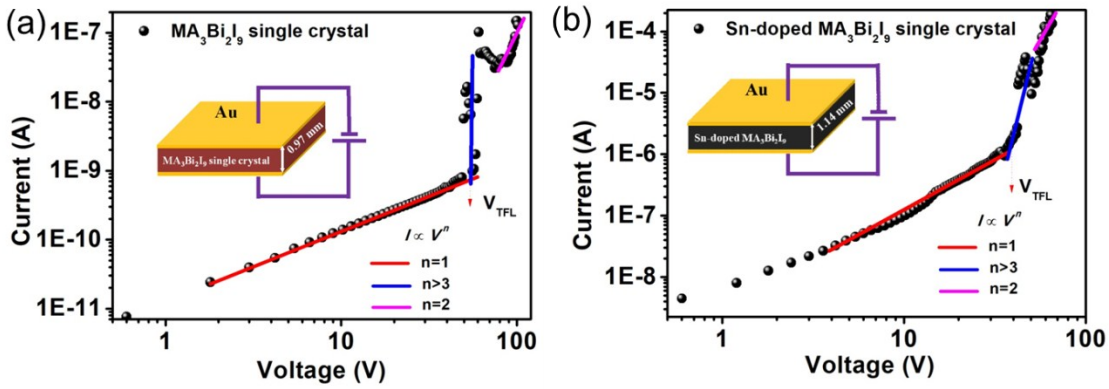

Fig. S10 (a) Dark current-voltage curve of $MA_3Bi_2I_9$ single crystal for space charge limited current analysis. (b) Dark current-voltage curve of Sn-doped $MA_3Bi_2I_9$ single crystal for space charge limited current analysis. The values of frequency, capacity, dielectric constant, trap-state density n_{trap} were listed into the following Table S3.

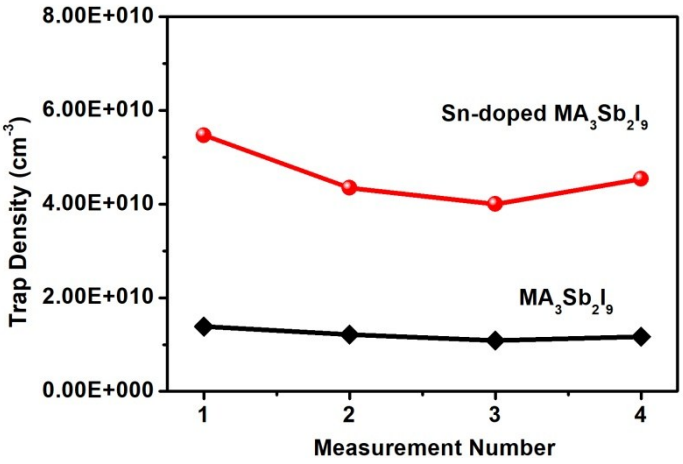

Fig. S11 The trap density of the samples measured by Hall Effect measurements.

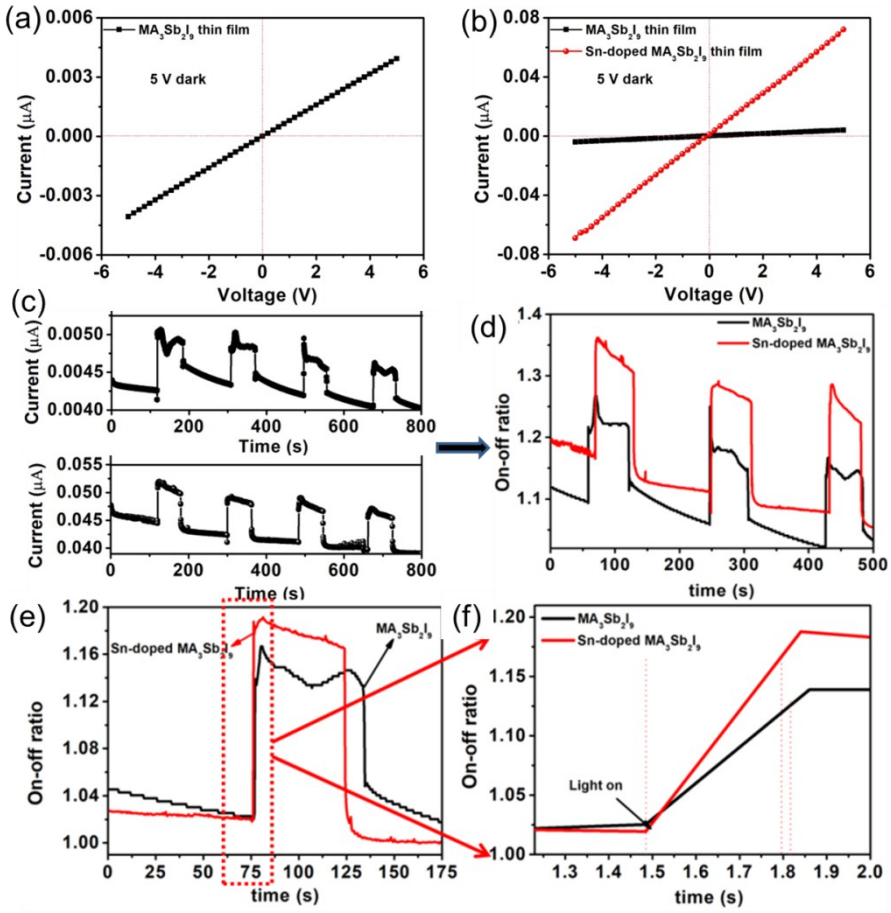

Fig. S12 (a, b) Dark current-voltage (I-V) curves of the photodetectors made of $MA_3Sb_2I_9$ and Sn-doped $MA_3Sb_2I_9$ thin film. (c-d) Photocurrent response and On-Off ratio for $MA_3Sb_2I_9$ and Sn-doped $MA_3Sb_2I_9$ thin film photodetectors under illumination at 20 mW using a laser emitting at 532 nm. (e) Photocurrent response time for $MA_3Sb_2I_9$ and Sn-doped $MA_3Sb_2I_9$ thin film photodetectors.

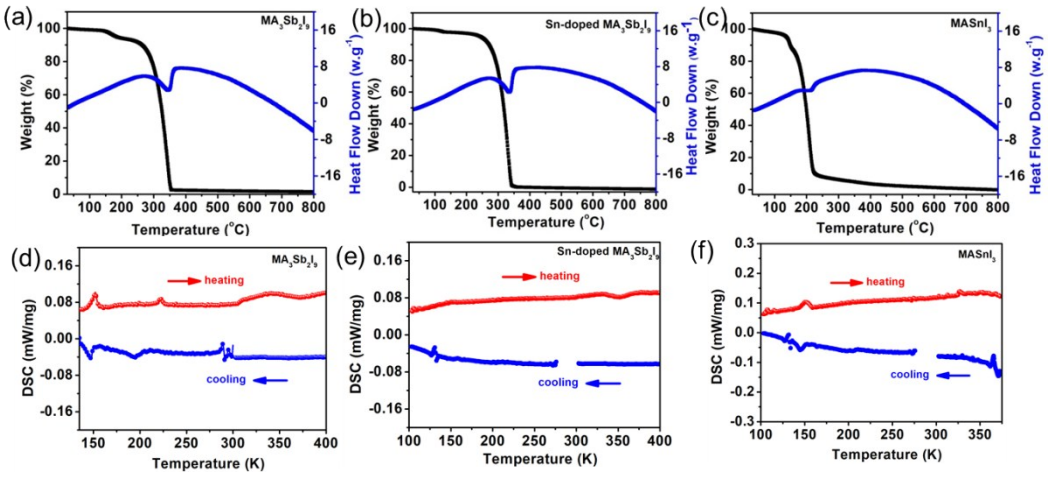

Fig. S13 (a-c) TGA and DSC data for the samples. The powder were placed in a platinum crucible, and heated at a rate of 10 °C min^{-1} from room temperature to 800 °C under flowing nitrogen gas. (c, d) The DSC curves with low temperature from 100 K to 400 K for $MA_3Sb_2I_9$, Sn-doped $MA_3Sb_2I_9$ and $MASnI_3$ single crystals.

Table S1. Chemical compositions of Sn-doped $MA_3Sb_2I_9$ determined X-ray fluorescence spectrometer (XRF).

Element	Result	Unit	Detectability	Element line	Intensity	w/o
Sn	20.7	mass%	0.13669	Sn-KA	13.0951	5.2306
Sb	79.3	mass%	0.13452	Sb-KA	37.9612	19.9926

Table S2. Crystal data and structure refinement for series of single crystals.

Empirical formula	$MA_3Sb_2I_9$	Sn-doped $MA_3Sb_2I_9$	$MASnI_3$
Formula weight/ g·mol^{-1}	1481.80	1481.80	531.46
Temperature/K	296	296	296
Wavelength/Å		0.71073	
Crystal color	fuchsia	black	black
Crystal system	Hexagonal	Hexagonal	Cubic
Space group	P63/mmc	P63/mmc	Pm-3m
a/Å	8.5508(10)	8.5699(8)	6.247(2)
b/Å	8.5508(10)	8.5699(8)	6.247(2)
c/Å	21.530(3)	21.552(2)	6.247(2)
α/°	90	90	90
β/°	90	90	90
γ/°	120	120	90
Volume/Å^3	1363.3 (4)	1370.8 (3)	243.8 (2)
Crystal size (mm^3)	0.15 × 0.15 × 0.09	0.23 × 0.12 × 0.03	0.18×0.17 × 0.13
Z	2	2	1
Density/g·cm^{-3}	3.434	3.391	3.497
μ(mm^{-1})	12.152	12.085	12.026
F (000)	1182.0	1172.0	216
Theta range (data collection)	2.75 to 26.09	2.74 to 26.03	3.26 to 27.53
Limiting indices	-11<=h<=11, -11<=k<=11, -27<=l<=27	-10<=h<=10, -10<=k<=10, -25<=l<=25	-7<=h<=7, -7<=k<=7, -7<=l<=7
GOF on F^2	1.230	1.204	1.238
Absorption correction	Semi-empirical from equivalents		
Data / restraints / parameters	644/ 0 / 17	508 /0 / 16	68/ 0 / 6

Table S3. The trap-state density of $MA_3Bi_2I_9$ and Sn-doped $MA_3Bi_2I_9$ single crystals at different frequencies.

	$MA_3Bi_2I_9$				Sn-doped $MA_3Bi_2I_9$			
Frequency (KHZ)	1	10	100	200	1	10	100	200
Capacity (pf)	1.33	1.22	1.16	1.15	1.05	0.89	0.83	0.82
dielectric constant ε	28.86	26.48	25.17	24.96	31.22	26.40	24.74	24.50
n_{trap} (cm^{-3})	1.89×10^{11}	1.73×10^{11}	1.64×10^{11}	1.63×10^{11}	1.04×10^{11}	8.79×10^{10}	8.26×10^{10}	8.18×10^{10}

References

(1) Hohenberg, P.; Kohn, W. Inhomogeneous Electron Gas. *Physical review* **1964**, *136* (3B), B864.

(2) Kohn, W.; Sham, L. J. Self-Consistent Equations Including Exchange and Correlation Effects. *Physical review* **1965**, *140* (4A), A1133.

(3) Giannozzi, P.; Baroni, S.; Bonini, N.; Calandra, M.; Car, R.; Cavazzoni, C.; Davide Ceresoli; Chiarotti, G. L.; Cococcioni, M.; Dabo, I.; et al. QUANTUM ESPRESSO: A Modular and Open-Source Software Project for Quantum Simulations of Materials. *J. Phys.: Condens. Matter* **2009**, *21* (39), 395502.

(4) Perdew, J. P.; Burke, K.; Ernzerhof, M. Generalized Gradient Approximation Made Simple. *Phys. Rev. Lett.* **1996**, *77* (18), 3865-3868.

(5) Sham, L. J.; Schlüter, M. Density-Functional Theory of the Energy Gap. *Phys. Rev. Lett.* **1983**, *51* (20), 1888-1891.

(6) Perdew, J. P.; Levy, M. Physical Content of the Exact Kohn-Sham Orbital Energies: Band Gaps and Derivative Discontinuities. *Phys. Rev. Lett.* **1983**, *51* (20), 1884-1887.

(7) Shishkin, M.; Kresse, G. Self-Consistent GW Calculations for Semiconductors and Insulators. *Phys. Rev. B* **2007**, *75* (23), 235102.

(8) Henderson, T. M.; Paier, J.; Scuseria, G. E. Accurate Treatment of Solids with the HSE Screened Hybrid. *phys. stat. sol. (b)* **2011**, *248* (4), 767-774.

(9) Monkhorst, H. J.; Pack, J. D. Special Points for Brillouin-Zone Integrations. *Phys. Rev. B* **1976**, *13* (12), 5188-5192.